

Direct observation of speed fluctuations of flagellar motor rotation at extremely low load close to zero

著者	Nakamura Shuichi, Hanaizumi Yuta, Morimoto Yusuke V., Inoue Yumi, Erhardt Marc, Minamino Tohru, Namba Keiichi
journal or publication title	Molecular microbiology
volume	113
number	4
page range	755-765
year	2019-12-11
URL	http://hdl.handle.net/10228/00007984

doi: <https://doi.org/10.1111/mmi.14440>

RESEARCH ARTICLE

Direct observation of speed fluctuations of flagellar motor rotation at extremely low load close to zero

Shuichi Nakamura ¹ | Yuta Hanaizumi¹ | Yusuke V. Morimoto ² | Yumi Inoue³ | Marc Erhardt ⁴ | Tohru Minamino ³ | Keiichi Namba ^{3,5,6}

¹Department of Applied Physics, Graduate School of Engineering, Tohoku University, Sendai, Japan

²Faculty of Computer Science and Systems Engineering, Department of Physics and Information Technology, Kyushu Institute of Technology, Fukuoka, Japan

³Graduate School of Frontier Biosciences, Osaka University, Osaka, Japan

⁴Institut für Biologie/Bakterienphysiologie, Humboldt-Universität zu Berlin, Berlin, Germany

⁵RIKEN Spring-8 Center and Center for Biosystems Dynamics Research, Osaka, Japan

⁶JEOL YOKOGUSHI Research Alliance Laboratories, Osaka University, Osaka, Japan

Correspondence

Shuichi Nakamura, Department of Applied Physics, Graduate School of Engineering, Tohoku University, 6-6-05 Aoba, Aoba-ku, Sendai, Miyagi 980-8579, Japan.
Email: naka@bp.apph.tohoku.ac.jp

Tohru Minamino and Keiichi Namba, Graduate School of Frontier Biosciences, Osaka University, 1-3 Yamadaoka, Suita, Osaka 565-0871, Japan.
Email: tohru@fbs.osaka-u.ac.jp (T. M.), keiichi@fbs.osaka-u.ac.jp (K. N.)

Present address

Yumi Inoue, Department of Ophthalmology and Visual Sciences, Kyoto University Graduate School of Medicine, Kyoto, Japan

Funding information

Japan Society for the Promotion of Science, Grant/Award Number: JP15H05593, JP24770141, JP25000013 and JP26293097; Ministry of Education, Culture, Sports, Science and Technology, Grant/Award Number: JP15H01335, JP24117004, JP25117501, JP25121718 and JP26115720

Abstract

The bacterial flagellar motor accommodates ten stator units around the rotor to produce large torque at high load. But when external load is low, some previous studies showed that a single stator unit can spin the rotor at the maximum speed, suggesting that the maximum speed does not depend on the number of active stator units, whereas others reported that the speed is also dependent on the stator number. To clarify these two controversial observations, much more precise measurements of motor rotation would be required at external load as close to zero as possible. Here, we constructed a *Salmonella* filament-less mutant that produces a rigid, straight, twice longer hook to efficiently label a 60 nm gold particle and analyzed flagellar motor dynamics at low load close to zero. The maximum motor speed was about 400 Hz. Large speed fluctuations and long pausing events were frequently observed, and they were suppressed by either over-expression of the MotAB stator complex or increase in the external load, suggesting that the number of active stator units in the motor largely fluctuates near zero load. We conclude that the lifetime of the active stator unit becomes much shorter when the motor operates near zero load.

KEYWORDS

bacterial flagellar motor, duty ratio, hook, MotAB stator complex, torque generation

1 | INTRODUCTION

Many bacteria utilize flagella to swim in aqueous environments and move on solid surfaces. The bacterial flagellum is composed of the membrane embedded basal body made of multiple rings and an axial structure consisting of the rod, the hook and the filament. The basal body is a rotary motor that drives the high-speed rotation of the helical filament as a propeller. The filament is a long helical tubular assembly of a single protein, flagellin and acts as a helical propeller to produce thrust to push the cell body forward. The rod is a straight and rigid tubular structure inside the basal body and functions as a drive shaft of the flagellar motor to transmit motor torque to the hook. The hook is highly curved and flexible in bending to work as a universal joint for smooth transmission of motor torque to the filament propeller (Minamino & Imada, 2015; Nakamura & Minamino, 2019).

The flagellar motor of *Escherichia coli* and *Salmonella* consists of a rotor and multiple stator units and is powered by proton motive force across the cytoplasmic membrane. The rotor is composed of the MS ring formed by the transmembrane protein FliF and the C ring consisting of three cytoplasmic proteins, FliG, FliM and FliN. The stator unit is made of two transmembrane proteins, MotA and MotB, and acts as a transmembrane proton channel to couple the energy of proton influx through the channel with torque generation (Berg, 2003; Morimoto & Minamino, 2014). Electrostatic interactions between MotA and FliG are involved in torque generation to drive the rotation of the flagellar motor (Morimoto, Nakamura, Hiraoka, Namba, & Minamino, 2013; Morimoto, Nakamura, Kami-ike, Namba, & Minamino, 2010; Zhou, Lloyd, & Blair, 1998). The association and dissociation cycle of MotA with FliG is coupled with inward-directed proton translocation through the transmembrane proton channel of the MotAB complex. Motor torque is believed to be generated by the following scheme: (a) proton from the cell exterior binds to a highly conserved Asp residue of MotB within the transmembrane proton channel (Asp-32 in *E. coli* MotB and Asp-33 in *Salmonella* MotB); (b) this proton-binding induces a conformational change of the MotAB stator complex, allowing MotA to interact with FliG on the rotor, forcing the rotor to move forward; (c) proton is released from

the proton channel to the cytoplasm and the MotAB stator complex dissociates from the rotor; (d) the stator conformation recovers to the free form (Minamino, Terahara, Kojima, & Namba, 2018).

To understand the torque generation mechanism of the flagellar motor, a variety of rotation assays have been carried out. In the earlier studies, slow rotation of the cell body caused by the attachment of a single flagellar filament to a glass surface via antibodies was measured (tethered cell assay) (Silverman & Simon, 1974). Then, rapid rotation of flagellar bundles in swimming bacteria was measured by analyzing the vibration frequency of the cell body (Lowe, Meister, & Berg, 1987). High-speed rotation and its fluctuation of a single flagellum was also measured by laser dark-field microscopy, showing that the *Salmonella* flagellar filament spins at around 170 Hz (Kudo, Magariyama, & Aizawa, 1990) and that the polar flagellar filament of *Vibrio alginolyticus* rotates at 1,700 Hz (Magariyama et al., 1994). Later, a single molecule technique using microbeads as a probe was established for much more precise measurements of flagellar motor rotation over a wide range of external load (Figure 1a) (Chen & Berg, 2000a, 2000b; Ryu, Berry, & Berg, 2000). In conventional bead assays, polystyrene beads (0.3–2.0 μm in diameter), fluorescent beads (40–200 nm) or gold nanoparticles (60–100 nm) are attached to partially sheared, sticky filaments lacking domain D3 domain of the filament protein flagellin (Yoshioka, Aizawa, & Yamaguchi, 1995), and then the rotation of the bead is recorded by a quadrant photodiode or a high-speed camera (Chen & Berg, 2000a, 2000b; Ryu et al., 2000). The torque versus speed relationship of the flagellar motor, namely torque-speed curve, has been clarified by this technique over a wide range of external load. The torque-speed curve comprises a high-load, low-speed regime exhibiting a substantially constant torque, and the low-load, high-speed regime showing a rather steep torque decline (Che et al., 2008; Chen & Berg, 2000a, 2000b; Nakamura, Kami-ike, et al., 2009; Nakamura, Kami-ike, Yokota, Minamino, & Namba, 2010; Nakamura, Morimoto, Kami-ike, Minamino, & Namba, 2009; Reid et al., 2006; Ryu et al., 2000; Sowa, Hotta, Homma, & Ishijima, 2003; Sowa et al., 2005). The flagellar motor of *E. coli* and *Salmonella* can accommodate about ten stator units around the rotor when the motor operates in the high-load, low-speed regime (Leake et al., 2006; Reid et al., 2006; Ryu et al., 2000). In contrast, the number of active stator units decreases from about

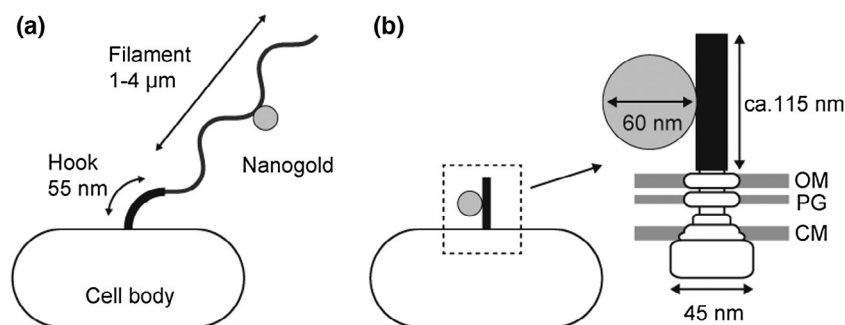


FIGURE 1 Rotation measurement of the flagellar motor using a nano-gold particle. (a) Conventional assay; a nano-gold particle is attached to a sticky filament stub. (b) Rotation assay using the *Salmonella* MMK2798iC strain, which produces 115 nm long, rigid, straight hooks without the filament attached; since each hook subunit of the straight hooks has three surface-exposed Cys residues, a nano-gold particle is directly attached to the long, rigid, straight and surface-thiolated hook. The outer membrane (OM), peptidoglycan layer (PG) and cytoplasmic membrane (CM) are indicated

ten to a few when the motor operates in the low-load, high-speed regime (Castillo et al., 2013; Chawla, Ford, & Lele, 2017; Lele, Hosu, & Berg, 2013; Nord, Gachon, et al., 2017; Pourjaberi, Terahara, Namba, & Minamino, 2017; Terahara, Noguchi, et al., 2017; Tipping, Delalez, Lim, Berry, & Armitage, 2013). Recently, it has also been shown that the number of active stators in the motor depends on the external concentration of coupling ions (Suzuki et al., 2019; Terahara, Kodera, et al., 2017). These observations suggest that the flagellar motor acts as a biosensor that detects changes in the environment to coordinate the number of active stator units around the rotor.

It has been shown that the maximum speed of the *E. coli* flagellar motor near zero load is constant even when the number of active stator units varies, suggesting that the duty ratio, which is defined as the fraction of time that a stator unit is involved in torque generation, is relatively large (Wang, Zhang, & Yuan, 2017; Yuan & Berg, 2008). In contrast, it has also been reported that the duty ratio of the flagellar motor is relatively small and that the maximum motor speed near zero load depends on the number of active stator units in the motor (Nord, Sowa, Steel, Lo, & Berry, 2017; Sato, Nakamura, Kudo, & Toyabe, 2019). To clarify these controversial observations, much more precise measurements of motor rotation would be required at external load as close to zero as possible. Even in bead assays with small gold nanoparticles (60–100 nm) attached to partially sheared, sticky filament stubs, the load by the rotation of the filament stub and relatively large radii of bead rotation is not negligibly small. Furthermore, the elasticity and flexibility of the filament and hook cause a prolonged relaxation time for the probe response, thereby hiding intrinsic motor dynamics.

To precisely measure flagellar motor dynamics at extremely low load close to zero, we decided to construct a *Salmonella* strain producing ~ 115 nm long, rigid, straight hook with three surface-exposed Cys residues to carry out bead assays using 60 nm gold particles (Figure 1b). The *Salmonella* hook protein FlgE shows considerable sequence and structural similarities to the distal rod protein FlgG (Chevance et al., 2007). FlgE consists of four domains, D0, Dc, D1 and D2 (Fujii, Kato, & Namba, 2009; Horváth, Kato, Miyata, & Namba, 2019), but FlgG is smaller than FlgE by lacking domain D2 (Chevance et al., 2007; Fujii et al., 2017). Intermolecular axial packing interactions between the D2 domains are responsible for hook supercoiling (Fujii, Matsunami, Inoue, & Namba, 2018; Kato, Makino, Miyata, Horváth, & Namba, 2019; Samatey et al., 2004), but those between Domain D2 and the triangular loop of domain D1 are dispensable for bending flexibility of the hook albeit important for the structural stability of the hook (Sakai, Inoue, Terahara, Namba, & Minamino, 2018). Both domain D2 and the triangular loop are absent in FlgG. Instead, domain Dc, which connects domains D0 and D1 in both FlgE and FlgG, contains a FlgG specific sequence (GSS) in FlgG consisting of 18 residues (YQTIHQPGAQSSEQTTLTP), not present in domain Dc of FlgE (Chevance et al., 2007; Fujii et al., 2017). An insertion of the GSS between Phe-42 and Ala-43 in domain Dc of FlgE makes the hook straight and rigid, indicating that the GSS confers the rigidity on the rod (Hiraoka et al., 2017). Therefore, we utilized not only this GSS insertion mutation but also the *fliC* null mutation

to remove the filament from the flagellar motor for high-resolution measurements of flagellar motor dynamics near zero load.

We show that the maximum motor speed near zero load reaches around 400 Hz and fluctuates considerably accompanied with frequent pausing events, leading to a conclusion that the zero-torque speed of the flagellar motor is also dependent on the number of active stator units in the motor and that the binding lifetime of each stator unit is quite short during high-speed rotation near zero load.

2 | RESULTS AND DISCUSSION

2.1 | Elongation of the rigid, straight hook

A *Salmonella* MME1001 (*flgE::GSS*, indicated as *flgE_{+GSS}*) strain, in which the GSS derived from the Dc region of FlgG is inserted between Phe-42 and Ala-43 of FlgE, produces rigid, straight hooks (Hiraoka et al., 2017). To directly label this straight hook with a 60 nm nano-gold particle, we replaced three surface-exposed residues, Thr-220, Thr-223, Thr-224 in domain D2 of FlgE_{+GSS}, by Cys residues (Supporting Information Figure S1). The hook length of the *Salmonella* flagellum is controlled at about 55 nm (Hirano, Yamaguchi, Oosawa, & Aizawa, 1994). However, the 55 nm long hook makes the labeling with a 60 nm nano-gold particle quite difficult. FliK acts as a secreted ruler protein to measure and determine the hook length during hook assembly (Erhardt et al., 2010; Erhardt, Singer, Wee, Keener, & Hughes, 2011; Minamino, González-Pedrajo, Yamaguchi, Aizawa, & Macnab, 1999; Minamino, Moriya, Hirano, Hughes, & Namba, 2009; Minamino et al., 2004; Moriya, Minamino, Hughes, Macnab, & Namba, 2006; Shibata et al., 2007). To make the straight hook much longer than the wild-type, we inserted residues 138–353 and residues 146–260 of YscP, which is a molecular ruler that determines the needle length of the *Yersinia* injectisome (Journet, Agrain, Broz, & Cornelis, 2003), between residues Thr-95 and Asp-96 and residues Leu-140 and Ser-141 in FliK respectively. Figure 2a is an electron micrograph of the hook isolated from the *Salmonella* mutant strain MMK2798iC. The length was elongated by these two insertions in FliK, but the diameter was the same as the wild-type hook in spite of the GSS insertion and cysteine substitutions (Supporting Information Figure S2). Precise measurements of the hook length showed that the length was distributed widely from 20 nm to 140 nm but with a main peak at 108 nm (Figure 2b). It has been shown that the insertion of GSS into FlgE reduces the rate of hook assembly significantly (Hiraoka et al., 2017). The balance between the polymerization rate of FlgE and the export ratio of FlgE over FliK affects the hook length (Inoue, Morimoto, Namba, & Minamino, 2018; Moriya et al., 2006), suggesting that the production of shorter hooks is presumably a consequence of a reduced polymerization rate of the straight hook. Based on the result of multi-Gaussian fitting to the length distribution, we split the data into longer and shorter groups; the average values and standard deviations of the longer and shorter groups were 115 ± 7 nm ($n = 78$, accounting for 64% of the data) and 59 ± 20 nm (36%) respectively (Figure 2b). Labeling of the shorter

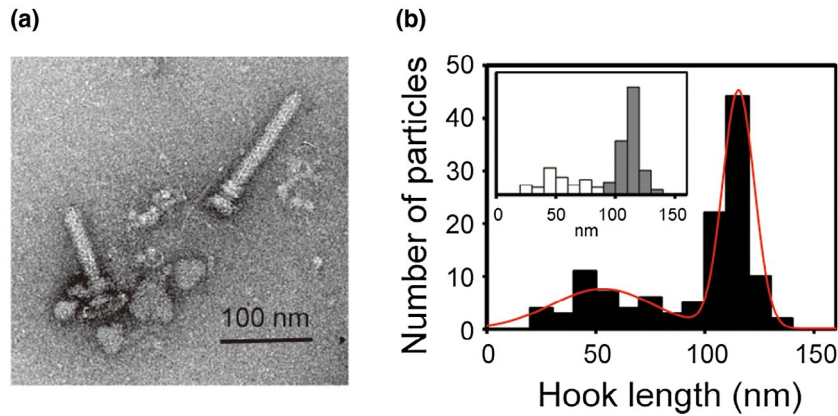


FIGURE 2 Hook length of the *Salmonella* MMK2798iC strain. (a) Electron micrograph of negatively stained hooks isolated from MMK2798iC cells. (b) Length distribution of the MMK2798iC hook ($n = 121$). Multi-Gaussian fitting to the histogram found peaks at 50 nm and 108 nm (red line). In the inset, the data are split into longer (>100 nm, gray) and shorter (<100 nm, white) groups; the average values and standard deviations of the longer and shorter groups are 115 ± 7 nm ($n = 78$) and 59 ± 20 nm ($n = 43$) respectively

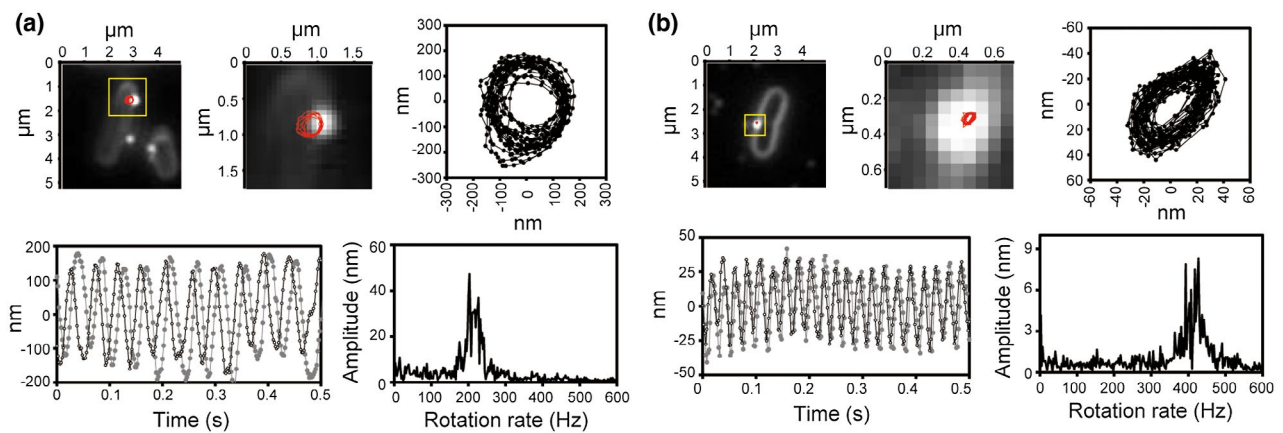


FIGURE 3 Rotation measurements near zero load. (a) The SJW46 cell with the sticky filament stub and (b) the MMK2798iC strain with the 115 nm long straight hook. (upper left) Image of bacterial cells and 60 nm gold particles attached to the hooks by optical microscopy with back-scattered light of laser illumination, with the rotation trajectory of a 60 nm gold particle in red; (upper middle) the region surrounded with a yellow square in the upper left panel is enlarged; (upper right) the rotation trajectory is extracted from the micrograph, with the center of the trajectory placed to the origin; (lower left) the time traces of the bead position in X (black) and Y (gray); (lower right) the power spectra showing peaks at around 200 Hz for SJW46 and around 400 Hz for MMK2798iC

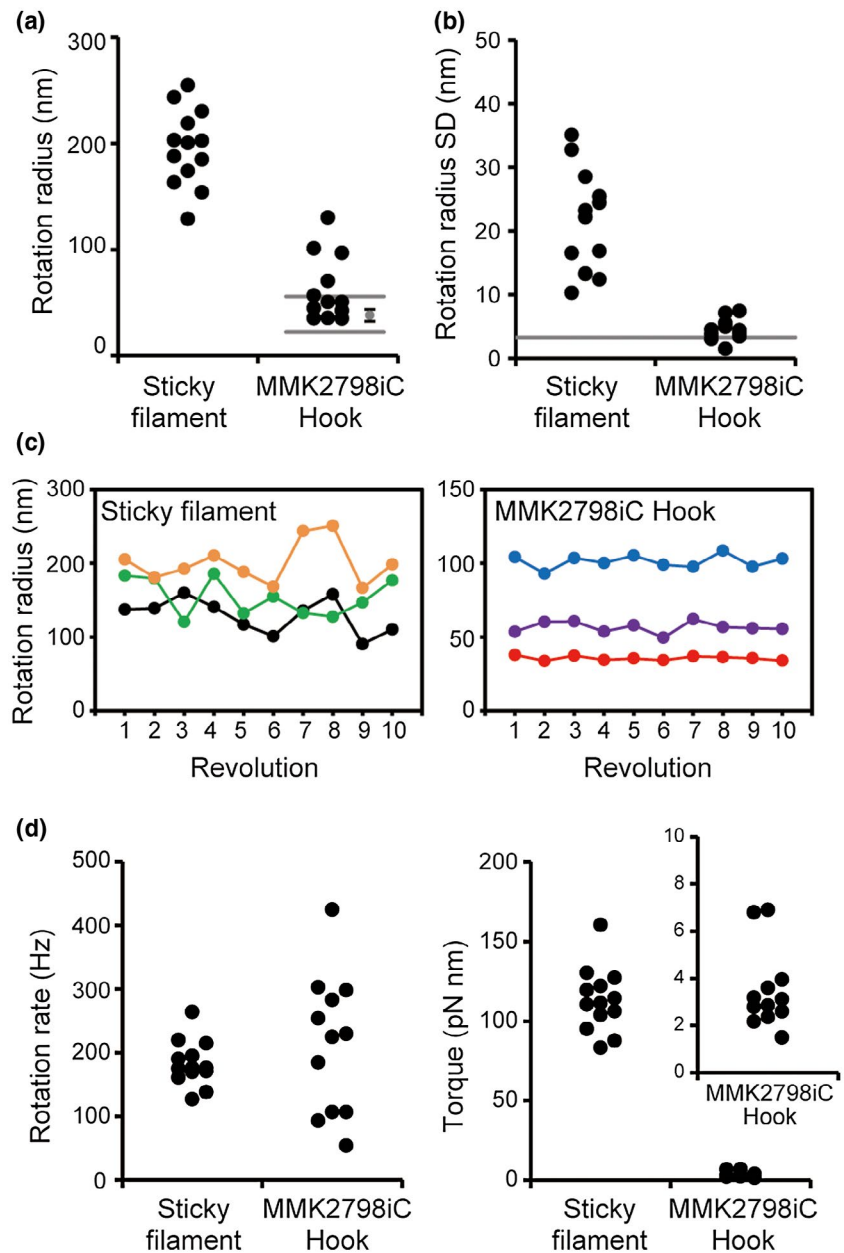
hook with a 60-nm gold bead may inhibit motor rotation due to the friction between the gold bead and the cell surface. Therefore, gold beads attached to ~ 115 nm hooks are those most likely measured by our bead assays.

2.2 | Rotation of a gold bead attached to the long, straight hook

We carried out two types of bead assays: in one, we labeled a 60 nm gold bead to the sticky filament stub of the *Salmonella* strain SJW46 (Figure 1a); in the other, to the 115 nm straight hook of the MMK2798iC strain, which does not produce the filament (Figure 1b). We measured their rotations at a frame rate of 5,000 Hz. Figure 3a,b show typical example data of motor rotation, with the sticky filament and the 115 nm straight hook respectively. The gold

bead attached to the sticky filament rotated with a rotation radius of about 150 nm (Figure 3a). In contrast, the rotation radius of the gold bead attached to the 115 nm straight hooks was about 40 nm (Figure 3b). The distributions of rotation radii are shown in Figure 4a. The rotation radii of gold beads attached to the sticky filaments and the 115 nm straight hooks were 196 ± 36 nm ($n = 13$ motors) and 63 ± 31 nm ($n = 12$ motors) respectively. The standard deviations of the rotation radii obtained from consecutive 10 rotations of individual motors are shown in Figure 4b. The standard deviations of the rotation radii of nano-gold particles attached to the rigid, straight hook without the filament were markedly smaller than those attached to the sticky filament and were even comparable to those of the gold beads directly attached to the glass surface, indicating the extremely stable rotation axis of the hook (≈ 3.3 nm; horizontal gray line in Figure 4b). This is also visualized in Figure 4c, where rotation radii of 10 revolutions were traced. The rotation axis of the hook

FIGURE 4 Intrinsic motor dynamics near zero load. (a) Rotation radii of 60 nm gold particles attached to the sticky filament stubs of SJW46 and the 115 nm straight hooks of MMK2798iC. The gray circle indicates the average rotation radius predicted from diameters of the gold particle and MMK2798iC hook; the horizontal gray lines indicates 3σ from the average value (see text for details). (b) Standard deviations (SD) of rotation radii of individual motors; values of SD were obtained from 10 consecutive revolutions in each motor. The horizontal gray line indicates SD of the position of a gold particle firmly attached to a glass surface ($= 3.3$ nm). (c) Trace of rotation radius determined for each revolution; data of three different motors are shown for each strain. (D) Rotation rate (left) and torque (right) of the motor with a 60 nm gold particle attached to the sticky filament stub or the 115 nm straight hook of MMK2798iC. The torque data of MMK2798iC is expanded in inset



was very stable with almost no fluctuation over multiple revolutions. These observations assure that the MMK2798iC strain producing the long, rigid, straight hook allows us to analyze the intrinsic motor dynamics at load extremely close to zero.

As mentioned above, the diameter of the straight hook produced by the MMK2798iC strain was the same as that of the wild-type hook (Supporting Information Figure S2). According to the data sheet provided from the manufacturer (BBI solutions), the mean diameter of nano-gold particle used in this study is 58.1 nm, and its variance is less than 8% (i.e., the standard deviation is 4.6 nm). If the bead assay of the MMK2798iC motor is modeled with a straight cylinder of 18 nm and an attached sphere of 58 nm in diameters as shown in Figure 1b, these geometrical values and the accuracy of the position in our measurement system predict that the rotation radius would be 38 ± 6 nm. In Figure 4a, this predicted value is shown by a gray circle (the error bar is the standard deviation), and 3σ from the mean value

are shown by horizontal gray lines. Because the rotations of the gold beads with rotation radii of about 100 nm (Figure 4a) were also stable (Figure 4b,c), their hooks are most likely rigid against bending and twisting but may still form a slightly curved tube due to possible intermolecular interactions of the D2 domains of FigE on the surface of the hook (Fujii et al., 2018; Kato et al., 2019; Samatey et al., 2004).

2.3 | Rotation rate and torque of the motor at extremely low load

Example data of 60 nm gold bead assays showed that the rotation rate of the motor with the sticky filament was about 200 Hz and that with the long, straight hook exceeded 400 Hz (Figure 3). Data plots of individual motors showed that the rotation rates of the motor with the sticky filament ranged from 120 to 260 Hz

($n = 13$ motors) while those with the long, straight hook distributed widely from 50 to 400 Hz ($n = 12$ motors) (Figure 4d, left panel). In a steady state of rotation, torque produced by the motor balances with a drag force by the fluid. Because the rotation rate of the flagellar motor $f = \omega/2\pi$, where ω is the angular velocity, is proportional to the motor torque M and inversely proportional to the drag coefficient γ , the value of M can be estimated from ω measured by bead assays and γ obtained theoretically from the shape parameters of the flagellar filament and probes: $M = \gamma \omega$. The motors with the sticky filaments produced torque around 120 pN nm, whereas those of the MMK2798iC motors with the long, straight hook produced torque that distributed from 1 to 7 pN nm, which is nearly two orders of magnitude smaller than the former (Figure 4d, right panel). When the 60 nm gold particle is attached to the sticky filament stub, which was shortened down to 1 μm in length and the rotational radius is 200 nm, the drag coefficient γ is $\sim 0.1\text{pN nm s}$; when the 60 nm gold is attached to the long, straight hook with a length of 115 nm and the rotation radius is 40 nm, the drag coefficient γ is $\sim 0.001\text{ pN nm s}$. This two orders of magnitude difference in the drag coefficient is in good agreement with the above torque values, indicating that we have achieved an extremely small external load condition for flagellar motor rotation measurements. We therefore conclude that the zero-torque speed of the *Salmonella* flagellar motor exceeds 400 Hz at zero load, which is much faster than any of the previous estimations (Nakamura, Kami-ike, et al., 2009; Nakamura et al., 2010).

Much larger speed fluctuations of the motor were observed at extremely small load compared to the motor with the sticky filament stub (Figure 4d). Interestingly, stepwise increases and decreases in the motor speed were quite often observed (Supporting Information Figure S3). Since the SJW46 motor has a short filament stub at the hook tip that increases the external load, even a small increase in the external load seems to suppress such speed fluctuations. Because the number of active stator units has been shown to vary from one to

five in the flagellar motor with a filament stub labeled with 100-nm gold bead (Lo, Sowa, Pilizota, & Berry, 2013), the variations of the rotation rate and torque of the SJW46 motor may be attributed to the difference in the number of active stator units in the motor. Since the maximum rotational speed of the *Salmonella* flagellar motor seems to depend on the number of active stator units around a rotor even at low load (Sato et al., 2019), we suggest that the number of active stator units largely fluctuates under the extremely low load condition achieved by the long, straight hook to cause large speed fluctuations. Because discrete speed ups and downs were quite often observed during rotation measurements at extremely low load close to zero (Supporting Information Figure S3), we conclude that the rotation rate of the flagellar motor operating in a low-load, high-speed regime depends on the number of functionally active stator units around the rotor and that the binding lifetime of each stator unit is relatively short as suggested before (Nord, Gachon, et al., 2017; Sato et al., 2019). But since the MotAB stator complex autonomously controls its proton channel activity in response to changes in external load (Che et al., 2014), it is also possible that the proton channel activity of the MotAB complex also fluctuates largely when the motor operates at zero load.

2.4 | Diffusive rotation of the motor at extremely low load

In the rotation measurements of the MMK2798iC motors with long, straight hooks, long pausing events were frequently observed (Figure 5a). Furthermore, we occasionally observed non-directional rotations of gold beads attached to their hooks during such pausing events (Figure 6a). The mean-square displacement (MSD) analysis of the non-directional rotations showed that the diffusion coefficient of the example data was $1,024\text{ rad}^2/\text{s}$ (Figure 6b). We examined whether the Brownian rotation motion of the MMK2798iC motor observed at extremely low load can be predicted theoretically.

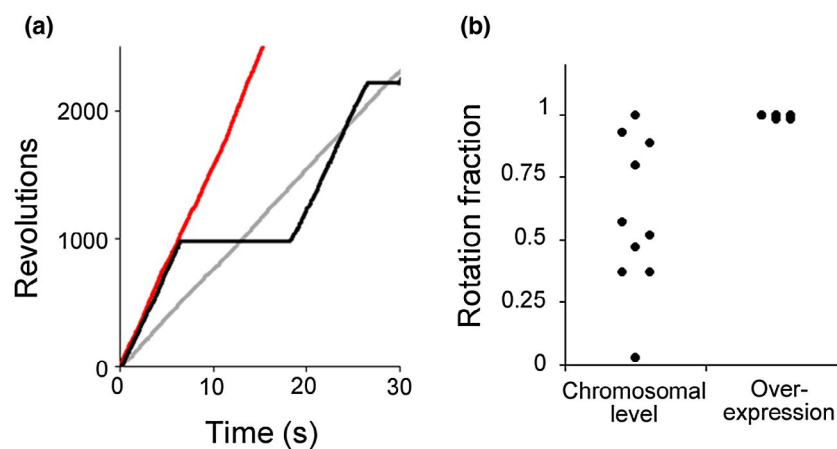


FIGURE 5 Effect of over-expression of the MotAB stator complex on pausing of the MMK2798iC motor. (a) Temporal rotation records of motors with a 60 nm gold particle attached to the 115 nm straight hook of the MMK2798iC cell and a 1 μm polystyrene bead attached to the sticky filament of SJW46 cell. Black line, chromosomal expression level of the MotAB complex in MMK2798iC; red line, over-expression of the MotAB complex in MMK2798iC; gray line, chromosomal expression level of the MotAB complex in SJW46. (b) The time fraction of rotation of the MMK2798iC motor at chromosomal and high expression levels of the MotAB stator complex; 10 motors were measured in each condition. The time fraction of each motor was the ratio of the summed rotation time to the total measurement time

FIGURE 6 Rotational diffusion of the flagellar motor without functional stator units. (a) Time-angle trace of diffusive motor rotation with a 60 nm gold particle attached to the MMK2798iC hook. The inset shows the X-Y trace for 0.5 s; the scale bar is 20 nm. (b) Mean-square displacement (MSD) analysis of the bead rotation shown in (a); the solid line is a regression line fitted to the MSD plot. (c) and (d) represent the parameters used for theoretical calculation of the diffusion constant based on the motor structure and the Einstein relation (see Experimental procedures); the ring structures comprising the basal body were assumed to be solid cylinders (right in d). Definitions of symbols and their values are shown in Table 1

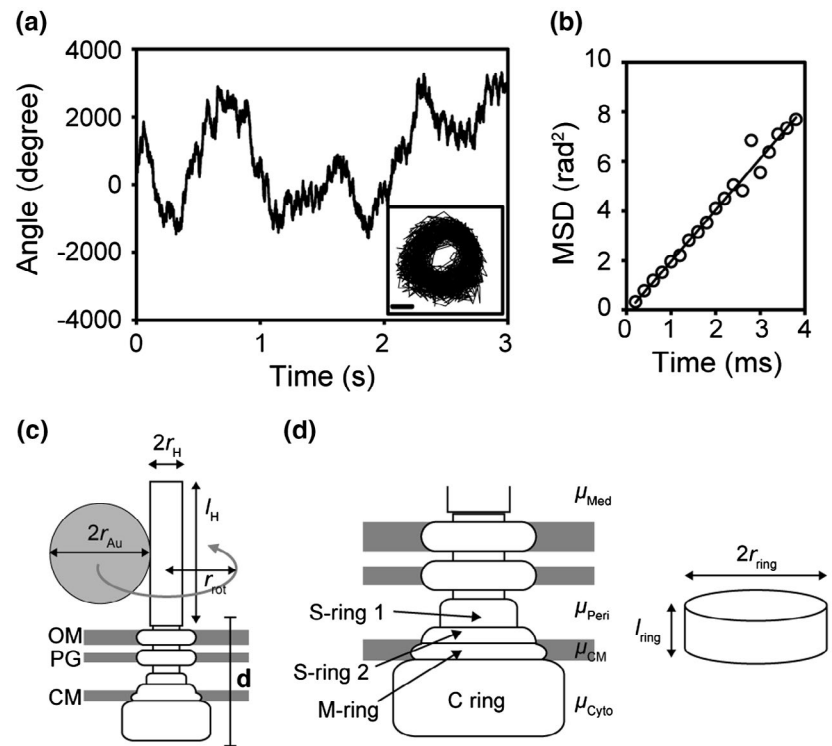


Figure 6c,d show schematics of the bead assay and flagellar basal body structure with the parameters used for derivation of the diffusion coefficient D of Brownian motion rotation (values of parameters are shown in Table 1). This model predicted that $D = 953 \text{ rad}^2/\text{s}$, which is in good agreement with the observed one above. This indicates that the non-directional rotation of the MMK2798iC motor results from the Brownian motion. Since free rotational diffusion has been reported for tethered *E. coli* cells expressing Na^+ -driven stator proteins upon removal of Na^+ from the solution to induce disassembly of the stator units from the motor (Sowa, Homma, Ishijima, & Berry, 2014), we suggest that the motors with such diffusive rotation do not contain active stator units around the rotor. Therefore, we propose that the continuous stator-rotor interactions coupled with proton translocation through the MotAB proton channel is required for the unidirectional rotation of the flagellar motor.

2.5 | Effect of over-expression of the stator unit on the pausing event

In contrast to the MMK2798iC motor rotation at extremely low load, long pausing events were never observed for the SJW46 motor with sticky filaments stub labeled with a 1 μm polystyrene bead (Figure 5a, grey line), raising the possibility that the dissociation rate of the stator unit is much faster under an extremely low load condition. If so, the over-expression of the MotAB stator complex would suppress such long pausing events. To examine this possibility, the rotation time was defined as the fraction of time that a motor spins over a certain period of time. When the MotAB complex was expressed from chromosomal DNA, the rotation times of the MMK2798iC motor varied from motor

to motor (Figure 5a, black line and b). In contrast, when the MotAB stator complex was overproduced, each single motor processively rotated (Figure 5a, red line and b). These results suggest that the lifetime of the active stator unit involved in torque generation is very short when the motor operates at extremely low load and that over-expression of the MotAB complex supports rapid and efficient stator installation into the motor from the membrane pool. The attachment of a short filament stub to the hook and a larger bead probe to the sticky filament stub suppress long pausing events of the flagellar motor (Figure 5a), suggesting that the lifetime of the active stator unit becomes much longer when the external load is high enough, and this is consistent with previous reports (Nord, Gachon, et al., 2017; Terahara, Kodera, et al., 2017). Since the dissociation rate of the stator unit from the rotor becomes much faster when the external load is extremely low, we conclude that at least a few active stator units are required for processive motor rotation at extremely low load close to zero as suggested before (Nord, Gachon, et al., 2017; Sato et al., 2019).

3 | EXPERIMENTAL PROCEDURES

3.1 | Bacterial strains and media

Salmonella enterica serovar Typhimurium strains SJW1103 (wild-type for motility and chemotaxis) (Yamaguchi, Fujita, Sugata, Taira, & Iino, 1984), SJW46 [*fliC*($\Delta 204$ -292)], which produces sticky filaments (Yoshioka et al., 1995), MME1001 (*flgE*::GSS, indicated as *flgE*_{+GSS}), which produces the straight hooks (Hiraoka et al., 2017) and EM2798 (*fliK22380*), of which FliK has insertions of residues 138-353 and residues 146-260 of YscP between residues Thr-95 and Asp-96 and

TABLE 1 Parameters used for simulation of free rotational diffusion of the hook basal body

Parameters	Symbols	Values	Position	References
Structure				
Filament length	l_F	1 μm	Medium	Che et al. (2008)
Filament diameter	$2r_F$	20 nm	Medium	Che et al. (2008)
Filament helix diameter	$2r_h$	0.4 μm	Medium	Che et al. (2008)
Filament helix pitch	p_h	2.3 μm	Medium	Che et al. (2008)
Hook length	l_H	115 nm	Medium	This study
Hook diameter	$2r_H$	20 nm	Medium	This study
Ring height				
S-ring 1	l_{S1}	6.5 nm	Periplasm	Fujii et al. (2017)
S-ring 2	l_{S2}	2.5 nm	Periplasm	Fujii et al. (2017)
M-ring	l_M	5.0 nm	Cytoplasmic membrane	Fujii et al. (2017)
C-ring	l_C	15.0 nm	Cytoplasm	Fujii et al. (2017)
Ring diameter				
S-ring 1	$2r_{S1}$	12.5 nm	Periplasm	Fujii et al. (2017)
S-ring 2	$2r_{S2}$	24.5 nm	Periplasm	Fujii et al. (2017)
M-ring	$2r_M$	30.0 nm	Cytoplasmic membrane	Fujii et al. (2017)
C-ring	$2r_C$	45.0 nm	Cytoplasm	Fujii et al. (2017)
Diameter of a gold bead	$2r_{Au}$	60 nm	Medium	
Viscosity				
Medium	μ_{Med}	0.97 mPa \times s		Castillo et al. (2013)
Periplasm	μ_{Peri}	34 mPa \times s		Mullineaux, Nennering, Ray, and Robinson (2006)
Cytoplasmic membrane	μ_{CM}	100 mPa \times s		Yuan and Berg (2008)
Cytoplasm	μ_{Cyto}	9.7 mPa \times s		Mullineaux et al. (2006)

residues Leu140 and Ser141 in FliK, respectively (Spöring et al., 2018), were used. We introduced the T220C/T223C/T224C triple mutation into the *flgE*_{+GSS} strain using the λ Red homologous recombination system (Datsenko & Wanner, 2000) to generate the MME1002 strain [*flgE*_{+GSS}(T220C/T223C/T224C)]. We transferred the *fliK22380* allele to the MME1002 strain by P22-mediated transduction, producing the MMK2798 strain [*flgE*_{+GSS}(T220C/T223C/T224C), *fliK22380*] and finally introduced the Δ *fliC::tetRA* allele into the MMK2798 strain to generate the MMK2798iC strain [*flgE*_{+GSS}(T220C/T223C/T224C), *fliK22380*, Δ *fliC::tetRA*]. DNA sequencing was carried out as described previously (Hara, Namba, & Minamino, 2011). L-broth (LB) and motility medium (pH 7.0) were prepared as described previously (Minamino, Imae, Oosawa, Kobayashi, & Oosawa, 2003; Minamino & Macnab, 1999).

3.2 | Measurements of hook length and diameter

Hook-basal bodies were purified from the *Salmonella* wild-type SJW1103 and MMK2798iC strains as described previously (Inoue et al., 2018). Samples were negatively stained with 2% (w/v) uranyl acetate. Electron micrographs were recorded with a JEM-1011 transmission electron microscope (JEOL, Tokyo, Japan) operated at 100 kV and equipped with a F415 CCD camera (TVIPS, Gauting,

Germany) at a magnification of $\times 5,500$, which corresponds to 2.75 nm per pixel. Hook length was measured by ImageJ version 1.48 (National Institutes of Health).

3.3 | Rotation assay

Rotation assays using the gold bead were performed as described previously with some modifications (Castillo et al., 2013; Che et al., 2008; Nakamura, Kami-ike, et al., 2009). SJW46 and MMK2789iC cells were grown overnight in LB at 37°C with shaking. Overnight culture was diluted 1:100 into fresh LB and incubated for 3 hr at 37°C. For SJW46, their sticky flagellar filaments were partially truncated by passing through a 25-gauge needle. After centrifugation, the cells were suspended into motility medium. MMK2798iC cells were washed by centrifugation, and then suspended into motility medium. The cell suspension was infused to a flow chamber and incubated for 20 min at 23°C. The cells floating in the chamber were removed by infusing motility medium and the motility medium containing gold beads with a diameter of 60 nm (BBI) was infused into the flow chamber and then incubated for 5 min at 23°C. Gold beads floating without attaching to partially truncated flagellar filaments or the hooks of MMK2798iC were removed by infusing motility medium. Rotations of gold beads were observed under a dark-field

microscope (BX53, 100 × oil immersion objective, 5 × relay lens; Olympus) and recorded by a high-speed CMOS (IDP-Express R2000, Photron) at a frame rate of 5,000 Hz. Data analysis was performed by a custom-made programs that we developed on the basis of LabVIEW 2014 (National Instruments).

For calculation of motor torque, the drag coefficients of the sticky filament labeled with gold beads γ_{F+Au} were obtained as described before (Sowa et al., 2003):

$$\gamma_{F+Au} = \gamma_F + \gamma_{Au} \quad (1)$$

$$\gamma_F = \frac{2\pi l_F r_h^2 (2p_h^2 + 4\pi^2 r_h^2) \mu_{Med}}{(p_h^2 + 4\pi^2 r_h^2) (\ln^{2p_h} / r_F - 0.5)} \quad (2)$$

$$\gamma_{Au} = 8\pi \mu_{Med} r_{Au}^3 + 6\pi \mu_{Med} r_{Au} r_{rot}^2 \quad (3)$$

Here, γ_F and γ_{Au} are drag coefficients of the flagellar filament and gold bead respectively; l_F , $2r_h$, p_h and $2r_F$ are the length, helix diameter, helix pitch and diameter of the filament respectively; $2r_{Au}$ and r_{rot} are the diameter and rotation radius of a gold bead respectively; μ_{Med} is viscosity of the motility medium. For the MMK2798iC motor, the straight hook was assumed to be a cylinder with a diameter of $2r_H$ and length of l_H and its drag coefficient γ_H was obtained as follows (Howard, 2001):

$$\gamma_H = 4\pi \mu_{Med} r_H^2 l_H \quad (4)$$

$$\gamma_{H+Au} = \gamma_H + \gamma_{Au} \quad (5)$$

Here, γ_{H+Au} is the drag coefficient of the MMK2798iC hook labeled with the gold bead. Values of parameters are described in Table 1.

3.4 | Theoretical estimation of the diffusion coefficient

The diffusion coefficient D of the modeled MMK2798iC motor with a 60 nm gold particle (Figure 5c,d) was derived by using the Einstein relation:

$$D = \frac{k_B T}{\gamma_{Model}} \quad (6)$$

$$\gamma_{Model} = \gamma_{Au} + \gamma_H + \gamma_{BB} \quad (7)$$

Here, k_B is the Boltzmann constant ($=1.38 \times 10^{-23}$ J/K), T is the absolute temperature ($=296$ K) and γ_{Model} is the drag coefficients of the motor labeled with the gold bead. The drag coefficient of the basal body γ_{BB} was obtained as follows:

$$\gamma_{BB} = \gamma_{S1} + \gamma_{S2} + \gamma_M + \gamma_C \quad (8)$$

$$\gamma_{S1} = 4\pi \mu_{Peri} r_{S1}^2 l_{S1} \quad (9)$$

$$\gamma_{S2} = 4\pi \mu_{Peri} r_{S2}^2 l_{S2} \quad (10)$$

$$\gamma_M = 4\pi \mu_{CM} r_M^2 l_M \quad (11)$$

$$\gamma_C = 4\pi \mu_{Cyto} r_C^2 l_C \quad (12)$$

Here, γ_{S1} , γ_{S2} , γ_M and γ_C are drag coefficients of S-ring 1, S-ring 2, M-ring and C-ring; μ_{Peri} , μ_{CM} and μ_{Cyto} are viscosities of the periplasmic space, cytoplasmic membrane and cytoplasm respectively. All of the ring structures were assumed as cylinders as with the hook; $2r$ and l are the diameter and length of the cylinder and rings are discriminated by subscripts. Values of parameters are described in Table 1.

ACKNOWLEDGEMENTS

We thank Nobunori Kami-ike and Koichi Hiraoka for technical supports. This work has been supported by MEXT KAKENHI Grant Number JP25117501 to S.N., JP26115720 and JP15H01335 to Y.V.M., JP24117004 and JP25121718 to T.M. and JSPS KAKENHI Grant number JP24770141 to S.N., JP15H05593 to Y.V.M., JP26293097 to T.M. and JP25000013 to K.N. This work has also been partially supported by JEOL YOKOGUSHI Research Alliance Laboratories of Osaka University to K.N. and by Platform Project for Supporting Drug Discovery and Life Science Research (BINDS) from AMED under Grant Number JP19am0101117 to K.N.

AUTHOR CONTRIBUTIONS

S.N., T.M. and K.N. designed research; S.N., Y.H., Y.V.M., Y.I., M.E. and T.M. performed research; S.N., Y.H., Y.I. and M.E. analyzed data; S.N., T.M. and K.N. wrote the paper based on discussion with other authors.

ORCID

Shuichi Nakamura  <https://orcid.org/0000-0003-3972-7779>

Yusuke V. Morimoto  <https://orcid.org/0000-0003-1573-8967>

Marc Erhardt  <https://orcid.org/0000-0001-6292-619X>

Tohru Minamino  <https://orcid.org/0000-0002-8175-1951>

Keiichi Namba  <https://orcid.org/0000-0003-2911-5875>

REFERENCES

- Berg, H. C. (2003). The rotary motor of bacterial flagella. *Annual Review of Biochemistry*, 72, 19–54. <https://doi.org/10.1146/annurev.biochem.72.121801.161737>
- Castillo, D. J., Nakamura, S., Morimoto, Y. V., Che, Y.-S., Kami-ike, N., Kudo, S., ... Namba, K. (2013). The C-terminal periplasmic domain of MotB is responsible for load-dependent control of the number of stators of the bacterial flagellar motor. *Biophysics*, 9, 173–181. <https://doi.org/10.2142/biophysics.9.173>
- Chawla, R., Ford, K. M., & Lele, P. P. (2017). Torque, but not FliL, regulates mechanosensitive flagellar motor-function. *Scientific Reports*, 7, 5565. <https://doi.org/10.1038/s41598-017-05521-8>
- Che, Y. S., Nakamura, S., Kojima, S., Kami-ike, N., Namba, K., & Minamino, T. (2008). Suppressor analysis of the MotB(D33E) mutation to probe the bacterial flagellar motor dynamics coupled with proton translocation. *Journal of Bacteriology*, 190, 6660–6667.

- Che, Y. S., Nakamura, S., Morimoto, Y. V., Kami-ike, N., Namba, K., & Minamino, T. (2014). Load-sensitive coupling of proton translocation and torque generation in the bacterial flagellar motor. *Molecular Microbiology*, *91*, 175–184. <https://doi.org/10.1111/mmi.12453>
- Chen, X., & Berg, H. C. (2000a). Torque-speed relationship of the flagellar rotary motor of *Escherichia coli*. *Biophysical Journal*, *78*, 1036–1041. [https://doi.org/10.1016/S0006-3495\(00\)76662-8](https://doi.org/10.1016/S0006-3495(00)76662-8)
- Chen, X., & Berg, H. C. (2000b). Solvent-isotope and pH effects on flagellar rotation in *Escherichia coli*. *Biophysical Journal*, *78*, 2280–2284. [https://doi.org/10.1016/S0006-3495\(00\)76774-9](https://doi.org/10.1016/S0006-3495(00)76774-9)
- Chevance, F. F., Takahashi, N., Karlinsey, J. E., Gnerer, J., Hirano, T., Samudrala, R., ... Hughes, K. T. (2007). The mechanism of outer membrane penetration by the eubacterial flagellum and implications for spirochete evolution. *Genes & Developments*, *21*, 2326–2335. <https://doi.org/10.1101/gad.1571607>
- Datsenko, K. A., & Wanner, B. L. (2000). One-step inactivation of chromosomal genes in *Escherichia coli* K-12 using PCR products. *Proceedings of the National Academy of Sciences of the United States of America*, *97*, 6640–6645. <https://doi.org/10.1073/pnas.120163297>
- Erhardt, M., Hirano, T., Su, Y., Paul, K., Wee, D. H., Mizuno, S., ... Hughes, K. T. (2010). The role of the FliK molecular ruler in hook-length control in *Salmonella enterica*. *Molecular Microbiology*, *75*, 1272–1284.
- Erhardt, M., Singer, H. M., Wee, D. H., Keener, J. P., & Hughes, K. T. (2011). An infrequent molecular ruler controls flagellar hook length in *Salmonella enterica*. *EMBO Journal*, *30*, 2948–2961.
- Fujii, T., Kato, T., Hiraoka, K. D., Miyata, T., Minamino, T., Chevance, F. F. V., ... Namba, K. (2017). Identical folds used for distinct mechanical functions of the bacterial flagellar rod and hook. *Nature Communications*, *8*, 14276. <https://doi.org/10.1038/ncomms14276>
- Fujii, T., Kato, T., & Namba, K. (2009). Specific arrangement of α -helical coiled coils in the core domain of the bacterial flagellar hook for the universal joint function. *Structure*, *17*, 1485–1493. <https://doi.org/10.1016/j.str.2009.08.017>
- Fujii, T., Matsunami, H., Inoue, Y., & Namba, K. (2018). Evidence for the hook supercoiling mechanism of the bacterial flagellum. *Biophysics and Physicobiology*, *15*, 28–32. https://doi.org/10.2142/biophysico.15.0_28
- Hara, N., Namba, K., & Minamino, T. (2011). Genetic characterization of conserved charged residues in the bacterial flagellar type III export protein FlhA. *PLoS ONE*, *6*, e22417. <https://doi.org/10.1371/journal.pone.0022417>
- Hirano, T., Yamaguchi, S., Oosawa, K., & Aizawa, S. (1994). Roles of FliK and FlhB in determination of flagellar hook length in *Salmonella typhimurium*. *Journal of Bacteriology*, *176*, 5439–5449. <https://doi.org/10.1128/jb.176.17.5439-5449.1994>
- Hiraoka, K. D., Morimoto, Y. V., Inoue, Y., Fujii, T., Miyata, T., Makino, F., ... Namba, K. (2017). Straight and rigid flagellar hook made by insertion of the FlgG specific sequence into FlgE. *Scientific Reports*, *7*, 46723. <https://doi.org/10.1038/srep46723>
- Horváth, P., Kato, T., Miyata, T., & Namba, K. (2019). Structure of *Salmonella* flagellar hook reveals intermolecular domain interactions for the universal joint function. *Biomolecules*, *9*, 462. <https://doi.org/10.3390/biom9090462>
- Howard, J. (2001). *Mechanics of motor proteins and the cytoskeleton*. Sunderland, MA: Sinauer.
- Inoue, Y., Morimoto, Y. V., Namba, K., & Minamino, T. (2018). Novel insights into the mechanism of well-ordered assembly of bacterial flagellar proteins in *Salmonella*. *Scientific Reports*, *8*, 1787. <https://doi.org/10.1038/s41598-018-20209-3>
- Journet, L., Agrain, C., Broz, P., & Cornelis, G. R. (2003). The needle length of bacterial injectisomes is determined by a molecular ruler. *Science*, *302*, 1757–1760. <https://doi.org/10.1126/science.1091422>
- Kato, T., Makino, F., Miyata, T., Horváth, P., & Namba, K. (2019). Structure of the native supercoiled flagellar hook as a universal joint. *Nature Communications*, *10*, 5295. <https://doi.org/10.1038/s41467-019-13252-9>
- Kudo, S., Magariyama, Y., & Aizawa, S.-I. (1990). Abrupt changes in flagellar rotation observed by laser dark-field microscopy. *Nature*, *346*, 677–680. <https://doi.org/10.1038/346677a0>
- Leake, M. C., Chandler, J. H., Wadhams, G. H., Bai, F., Berry, R. M., & Armitage, J. P. (2006). Stoichiometry and turnover in single, functioning membrane protein complexes. *Nature*, *443*, 355–358. <https://doi.org/10.1038/nature05135>
- Lele, P. P., Hosu, B. G., & Berg, H. C. (2013). Dynamics of mechanosensing in the bacterial flagellar motor. *Proceedings of the National Academy of Sciences of the United States of America*, *110*, 11839–11844. <https://doi.org/10.1073/pnas.1305885110>
- Lo, C.-J., Sowa, Y., Pilizota, T., & Berry, R. M. (2013). Mechanism and kinetics of a sodium-driven bacterial flagellar motor. *Proceedings of the National Academy of Sciences of the United States of America*, *110*, E2544–E2551. <https://doi.org/10.1073/pnas.1301664110>
- Lowe, G., Meister, M., & Berg, H. C. (1987). Rapid rotation of flagellar bundles in swimming bacteria. *Nature*, *325*, 637–640. <https://doi.org/10.1038/325637a0>
- Magariyama, Y., Sugiyama, S., Muramoto, K., Maekawa, Y., Kawagishi, I., Imae, Y., & Kudo, S. (1994). Very fast flagellar rotation. *Nature*, *371*, 752. <https://doi.org/10.1038/371752b0>
- Minamino, T., González-Pedrajo, B., Yamaguchi, K., Aizawa, S.-I., & Macnab, R. M. (1999). FliK, the protein responsible for flagellar hook length control in *Salmonella*, is exported during hook assembly. *Molecular Microbiology*, *34*, 295–304. <https://doi.org/10.1046/j.1365-2958.1999.01597.x>
- Minamino, T., & Imada, K. (2015). The bacterial flagellar motor and its structural diversity. *Trends in Microbiology*, *23*, 267–274. <https://doi.org/10.1016/j.tim.2014.12.011>
- Minamino, T., Imae, Y., Oosawa, F., Kobayashi, Y., & Oosawa, K. (2003). Effect of intracellular pH on rotational speed of bacterial flagellar motors. *Journal of Bacteriology*, *185*, 1190–1194. <https://doi.org/10.1128/JB.185.4.1190-1194.2003>
- Minamino, T., & Macnab, R. M. (1999). Components of the *Salmonella* flagellar export apparatus and classification of export substrates. *Journal of Bacteriology*, *181*, 1388–1394.
- Minamino, T., Moriya, N., Hirano, T., Hughes, K. T., & Namba, K. (2009). Interaction of FliK with the bacterial flagellar hook is required for efficient export specificity switching. *Molecular Microbiology*, *74*, 239–251. <https://doi.org/10.1111/j.1365-2958.2009.06871.x>
- Minamino, T., Saijo-Hamano, Y., Furukawa, Y., González-Pedrajo, B., Macnab, R. M., & Namba, K. (2004). Domain organization and function of *Salmonella* FliK, a flagellar hook-length control protein. *Journal of Molecular Biology*, *341*, 491–502. <https://doi.org/10.1016/j.jmb.2004.06.012>
- Minamino, T., Terahara, N., Kojima, S., & Namba, K. (2018). Autonomous control mechanism of stator assembly in the bacterial flagellar motor in response to changes in the environment. *Molecular Microbiology*, *109*, 723–734. <https://doi.org/10.1111/mmi.14092>
- Morimoto, Y. V., & Minamino, T. (2014). Structure and function of the bi-directional bacterial flagellar motor. *Biomolecules*, *4*, 217–234. <https://doi.org/10.3390/biom4010217>
- Morimoto, Y. V., Nakamura, S., Hiraoka, K. D., Namba, K., & Minamino, T. (2013). Distinct roles of highly conserved charged residues at the MotA-FliG interface in bacterial flagellar motor rotation. *Journal of Bacteriology*, *195*, 474–481. <https://doi.org/10.1128/JB.01971-12>
- Morimoto, Y. V., Nakamura, S., Kami-ike, N., Namba, K., & Minamino, T. (2010). Charged residues in the cytoplasmic loop of MotA are required for stator assembly into the bacterial flagellar motor. *Molecular Microbiology*, *78*, 1117–1129. <https://doi.org/10.1111/j.1365-2958.2010.07391.x>
- Moriya, N., Minamino, T., Hughes, K. T., Macnab, R. M., & Namba, K. (2006). The type III flagellar export specificity switch is dependent

- on FliK ruler and a molecular clock. *Journal of Molecular Biology*, 359, 466–477. <https://doi.org/10.1016/j.jmb.2006.03.025>
- Mullineaux, C. W., Nenner, A., Ray, N., & Robinson, C. (2006). Diffusion of green fluorescent protein in three cell environments in *Escherichia coli*. *Journal of Bacteriology*, 188, 3442–3448. <https://doi.org/10.1128/JB.188.10.3442-3448.2006>
- Nakamura, S., Kami-ike, N., Yokota, J. P., Kudo, S., Minamino, T., & Namba, K. (2009). Effect of intracellular pH on the torque-speed relationship of bacterial proton-driven flagellar motor. *Journal of Molecular Biology*, 386, 332–338. <https://doi.org/10.1016/j.jmb.2008.12.034>
- Nakamura, S., Kami-ike, N., Yokota, J. P., Minamino, T., & Namba, K. (2010). Evidence for symmetry in the elementary process of bidirectional torque generation by the bacterial flagellar motor. *Proceedings of the National Academy of Sciences of the United States of America*, 107, 17616–17620. <https://doi.org/10.1073/pnas.1007448107>
- Nakamura, S., & Minamino, T. (2019). Flagella-driven motility of bacteria. *Biomolecules*, 9, 279. <https://doi.org/10.3390/biom9070279>
- Nakamura, S., Morimoto, Y. V., Kami-ike, N., Minamino, T., & Namba, K. (2009). Role of a conserved prolyl residue (Pro-173) of MotA in the mechanochemical reaction cycle of the proton-driven flagellar motor of *Salmonella*. *Journal of Molecular Biology*, 393, 300–307. <https://doi.org/10.1016/j.jmb.2009.08.022>
- Nord, A. L., Gachon, E., Perez-Carrasco, R., Nirody, J. A., Barducci, A., Berry, R. M., & Pedaci, F. (2017). Catch bond drives stator mechanosensitivity in the bacterial flagellar motor. *Proceedings of the National Academy of Sciences of the United States of America*, 114, 12952–12957. <https://doi.org/10.1073/pnas.1716002114>
- Nord, A. L., Sowa, Y., Steel, B. C., Lo, C.-J., & Berry, R. M. (2017). Speed of the bacterial flagellar motor near zero load depends on the number of stator units. *Proceedings of the National Academy of Sciences of the United States of America*, 114, 11603–11608. <https://doi.org/10.1073/pnas.1708054114>
- Pourjaberi, S. N. S., Terahara, N., Namba, K., & Minamino, T. (2017). The role of a cytoplasmic loop of MotA in load-dependent assembly and disassembly dynamics of the MotA/B stator complex in the bacterial flagellar motor. *Molecular Microbiology*, 106, 646–658. <https://doi.org/10.1111/mmi.13843>
- Reid, S. W., Leake, M. C., Chandler, J. H., Lo, C. J., Armitage, J. P., & Berry, R. M. (2006). The maximum number of torque-generating units in the flagellar motor of *Escherichia coli* is at least 11. *Proceedings of the National Academy of Sciences of the United States of America*, 103, 8066–8071. <https://doi.org/10.1073/pnas.0509932103>
- Ryu, W. S., Berry, R. M., & Berg, H. C. (2000). Torque-generating units of the flagellar motor of *Escherichia coli* have a high duty ratio. *Nature*, 403, 444–447. <https://doi.org/10.1038/35000233>
- Sakai, T., Inoue, Y., Terahara, N., Namba, K., & Minamino, T. (2018). A triangular loop of domain D1 of FlgE is essential for hook assembly but not for the mechanical function. *Biochemical and Biophysical Research Communications*, 495, 1789–1794. <https://doi.org/10.1016/j.bbrc.2017.12.037>
- Samatey, F. A., Matsunami, H., Imada, K., Nagashima, S., Shaikh, T. R., Thomas, D. R., ... Namba, K. (2004). Structure of the bacterial flagellar hook and implication for the molecular universal joint mechanism. *Nature*, 431, 1062–1068. <https://doi.org/10.1038/nature02997>
- Sato, K., Nakamura, S., Kudo, S., & Toyabe, S. (2019). Evaluation of the duty ratio of the bacterial flagellar motor by dynamic load control. *Biophysical Journal*, 116, 1952–1959. <https://doi.org/10.1016/j.bpj.2019.04.004>
- Shibata, S., Takahashi, N., Chevance, F. F. V., Karlinsky, J. E., Hughes, K. T., & Aizawa, S.-I. (2007). FliK regulates flagellar hook length as an internal ruler. *Molecular Microbiology*, 64, 1404–1415. <https://doi.org/10.1111/j.1365-2958.2007.05750.x>
- Silverman, M., & Simon, M. (1974). Flagellar rotation and the mechanism of bacterial motility. *Nature*, 249, 73–74. <https://doi.org/10.1038/249073a0>
- Sowa, Y., Homma, M., Ishijima, A., & Berry, R. M. (2014). Hybrid-fuel bacterial flagellar motors in *Escherichia coli*. *Proceedings of the National Academy of Sciences of the United States of America*, 111, 3436–3441.
- Sowa, Y., Hotta, H., Homma, M., & Ishijima, A. (2003). Torque-speed relationship of the Na⁺-driven flagellar motor of *Vibrio alginolyticus*. *Journal of Molecular Biology*, 327, 1043–1051. [https://doi.org/10.1016/S0022-2836\(03\)00176-1](https://doi.org/10.1016/S0022-2836(03)00176-1)
- Sowa, Y., Rowe, A. D., Leake, M. C., Yakushi, T., Homma, M., Ishijima, A., & Berry, R. M. (2005). Direct observation of steps in rotation of the bacterial flagellar motor. *Nature*, 437, 916–919. <https://doi.org/10.1038/nature04003>
- Spöring, I., Martinez, V. A., Hotz, C., Schwarz-Linek, J., Grady, K. L., Nava-Sedeño, J. M., ... Erhardt, M. (2018). Hook length of the bacterial flagellum is optimized for maximal stability of the flagellar bundle. *PLOS Biology*, 16, e2006989. <https://doi.org/10.1371/journal.pbio.2006989>
- Suzuki, Y., Morimoto, Y. V., Oono, K., Hayashi, F., Oosawa, K., Kudo, S., & Nakamura, S. (2019). Effect of the MotA(M206I) mutation on torque generation and stator assembly in the *Salmonella* H⁺-driven flagellar motor. *Journal of Bacteriology*, 201, e00727-18.
- Terahara, N., Kodera, N., Uchihashi, T., Ando, T., Namba, K., & Minamino, T. (2017). Na⁺-induced structural transition of MotPS stator assembly of the *Bacillus* flagellar motor. *Science Advances*, 3, eaao4119.
- Terahara, N., Noguchi, Y., Nakamura, S., Kami-ike, N., Ito, M., Namba, K., & Minamino, T. (2017). Load- and polysaccharide-dependent activation of the Na⁺-type MotPS stator in the *Bacillus subtilis* flagellar motor. *Scientific Reports*, 7, 46081.
- Tipping, M. J., Delalez, N. J., Lim, R., Berry, R. M., & Armitage, J. P. (2013). Load-dependent assembly of the bacterial flagellar motor. *mBio*, 4, e00551-13. <https://doi.org/10.1128/mBio.00551-13>
- Wang, B., Zhang, R., & Yuan, J. (2017). Limiting (zero-load) speed of the rotary motor of *Escherichia coli* is independent of the number of torque-generating units. *Proceedings of the National Academy of Sciences of the United States of America*, 114, 12478–12482.
- Yamaguchi, S., Fujita, H., Sugata, K., Taira, T., & Iino, T. (1984). Genetic analysis of H2, the structural gene for phase-2 flagellin in *Salmonella*. *Journal of General Microbiology*, 130, 255–265.
- Yoshioka, K., Aizawa, S.-I., & Yamaguchi, S. (1995). Flagellar filament structure and cell motility of *Salmonella typhimurium* mutants lacking part of the outer domain of flagellin. *Journal of Bacteriology*, 177, 1090–1093. <https://doi.org/10.1128/jb.177.4.1090-1093.1995>
- Yuan, J., & Berg, H. C. (2008). Resurrection of the flagellar rotary motor near zero load. *Proceedings of the National Academy of Sciences of the United States of America*, 105, 1182–1185. <https://doi.org/10.1073/pnas.0711539105>
- Zhou, J., Lloyd, S. A., & Blair, D. F. (1998). Electrostatic interactions between rotor and stator in the bacterial flagellar motor. *Proceedings of the National Academy of Sciences of the United States of America*, 95, 6436–6441. <https://doi.org/10.1073/pnas.95.11.6436>

SUPPORTING INFORMATION

Additional supporting information may be found online in the Supporting Information section.

How to cite this article: Nakamura S, Hanaizumi Y, Morimoto YV, et al. Direct observation of speed fluctuations of flagellar motor rotation at extremely low load close to zero. *Mol Microbiol*. 2019;00:1–11. <https://doi.org/10.1111/mmi.14440>